Stowing strategy for a heliostat field based on wind speed and direction

Cite as: AIP Conference Proceedings **2445**, 120011 (2022); https://doi.org/10.1063/5.0085677
Published Online: 12 May 2022

Matthew Emes, Azadeh Jafari, Mike Collins, et al.

Stowing Strategy for a Heliostat Field Based on Wind Speed and Direction

Matthew Emes[1, a)], Azadeh Jafari[1, b)], Mike Collins[2, c)], Stefan Wilbert[3, d)], Luis Zarzalejo[4, e)], Silvan Siegrist[5, f)] and Maziar Arjomandi[1, g)]

[1]*Centre for Energy Technology, School of Mechanical Engineering, The University of Adelaide, Adelaide, SA 5005, Australia*
[2]*CSIRO Energy, 10 Murray Dwyer Circuit, Mayfield West, NSW 2304, Australia*
[3]*German Aerospace Center (DLR), Institute of Solar Research, Paseo de Almería 73, 04001 Almería, Spain*
[4]*Centro de Investigaciones Energéticas, Medioambientales y Tecnológicas (CIEMAT), División de Energías Renovables, Avda. Complutense 40, 28040 Madrid, Spain*
[5]*Lumoview Building Analytics GmbH, Im Mediapark 5, 50670 Köln, Germany*

[a)]Corresponding author: matthew.emes@adelaide.edu.au
[b)]azadeh.jafari@adelaide.edu.au
[c)]mike.collins@csiro.au
[d)]stefan.wilbert@dlr.de
[e)]lf.zarzalejo@ciemat.es
[f)]silvan.siegrist@lumoview.com
[g)]maziar.arjomandi@adelaide.edu.au

Abstract. This paper investigates a stowing strategy of a heliostat field based on wind speed and direction, in terms of the potential benefit of additional energy collection through the partial stowing of heliostats within an azimuth angle range with reduced operating wind loads. Correlations of one-minute wind speed and DNI at a heliostat field site with the operating wind loads, based on the azimuth-elevation tracking angles of individual heliostats, were used to assess the increased operating time and collected thermal energy by the field. The results show that more than 23% of heliostats in the sector of the field with operating wind loads that are smaller than 50% of the stow loads can continue to operate during a high-wind period (e.g. 10 m/s). Adopting a stow strategy based on wind direction can increase the annual operating time of the heliostat field by 6% with increasing stow design wind speed from 6 m/s to 12 m/s. Furthermore, the stowing strategy based on wind direction to allow heliostats to continue to operate at wind speeds exceeding 10 m/s can achieve an additional 280 MWh of thermal energy collected by the heliostat field operation during time periods that would conventionally stow the entire field with 24 GWh of annual thermal energy captured.

INTRODUCTION

The heliostat field represents the largest contribution and almost half of the total capital cost of a concentrating solar thermal power tower plant [1, 2]. Design specifications for the operating conditions of a heliostat field affect the performance and cost of a concentrating solar thermal power tower plant. The heliostat structural components, including the pedestal and torque tube, account for 18-34% of the total cost of conventional T-shaped heliostats depending on the heliostat size [3]. Furthermore, the drive unit represents 35-50% of the heliostat cost [3] to effectively track over a range of required motions and reflect the sunlight onto a receiver at the top of a tower during operation of the plant. Spillage losses due to wind-induced tracking errors become significant on heliostats with increasing distance from the tower, however the operating range of elevation and azimuth angles is typically larger for heliostats closer to the tower. By reducing the azimuth angle range from 180° to 140°, the estimated total energy loss of 3% can be compensated by an increase of 4% of the number of heliostats in the field [4].

SolarPACES 2020
AIP Conf. Proc. 2445, 120011-1–120011-8; https://doi.org/10.1063/5.0085677
Published by AIP Publishing. 978-0-7354-4195-8/$30.00

The cost of conventional heliostat drives can be effectively reduced with an accurate estimation of the wind loading for the expected range of elevation and azimuth angles of heliostats during operation of a field. For instance, the elevation angle varies between 13° and 77° during operation of heliostats located at the edge of a 150 MW field, containing 35,000 heliostats distributed over a radius of 500 m in a surround field arrangement [5]. Furthermore, the elevation angles of two heliostats positioned at radial distance of 100 m and 362 m from a 100-m tower can differ by up to 15° when tracking throughout a day [6]. The specifications for the operation of a heliostat field include a threshold (design) wind speed at which the heliostats are moved to stow position. Standard practice in the operation of heliostat fields is to stow the entire field during the approach of a high-wind event, such as gust front when the wind speed exceeds this design wind speed. The peak wind loads on heliostats in some operating positions exceed the maximum stow load, depending on the azimuth-elevation configuration of the heliostat and the turbulence intensity and length scales in the atmospheric boundary layer (ABL) simulated in wind tunnel experiments on scale-model heliostats at the University of Adelaide [3, 7-12]. It has be shown that the maximum wind loading on the drives and supporting structure during a synoptic gust front with a steady wind direction only applies to a portion of the heliostats in the field, such as azimuth angles of 0° (wind impacting front of heliostat) and 180° (wind impacting back of heliostat) for the hinge moment and overturning moment, and azimuth angles of ±60° and ±120° for the azimuth moment [8]. In this study, a strategy that stows heliostats based on a design wind speed and wind direction is investigated through a sensitivity analysis of the azimuth angles of individual heliostats within a field and their corresponding aerodynamic load coefficients derived in wind tunnel experiments. The current study aims to investigate the maximum operating loads and survival stow loads on multiple 39.6 m^2 heliostats in the 7 MW$_{th}$ CESA-I field, through the correlation of:

1. Historical wind speed and DNI data measurements by the German Aerospace Center (DLR) Institute of Solar Research and Centro de Investigaciones Energéticas, Medioambientales y Tecnológicas (CIEMAT) at CIEMAT's Plataforma Solar de Almeria (PSA) in Spain.
2. Non-dimensional wind load coefficients on a scale-model heliostat [3, 7, 8] at a range of elevation (α) and azimuth (β) angles in the University of Adelaide wind tunnel.

The outcomes of the present study provide an understanding of the daily and seasonal variation of the design wind loads on individual heliostats and the influence of wind direction on the loading distribution throughout a polar heliostat field, such that there is a potential to increase the operating minutes of protected regions of the heliostat field and thus maximize the energy yield of a power tower plant. Collection of high-fidelity wind velocity measurements over extended periods (i.e. years) can improve the annual operating time and efficiency of the heliostat field thermal energy capture at concentrating solar power plant sites, through the improved resolution of operating load data.

METHODOLOGY

Wind velocity measurements were obtained by a single CSAT3 ultrasonic anemometer at a 4.5-m height, mounted alongside three cup anemometers and a vane anemometer (Figure 1b) on a 10-m height meteorological mast (37.094° N, 2.359° W) to the east of the 7 MW$_{th}$ (5 MW$_e$) CESA-I heliostat field (Figure 1a) at PSA. The terrain surrounding the PSA site was characterized to approximate an open country terrain with a logarithmic law surface roughness height $z_0 = 0.08$ m and turbulence intensities $I_u = 25\%$ and $I_w = 12\%$ in the longitudinal and vertical directions, respectively [5, 13]. Analysis of the one-minute wind speed distribution (Figure 2a) in the year of 2016 showed that wind speeds above 10 m/s approached the CESA-I heliostat field from westerly and easterly directions (clockwise angle from north in Figure 2b), in agreement with previous analysis of wind speeds over 30 m/s over several years [5]. When correlating wind speed with the heliostat field operating time, during daytime minutes with DNI > 300 W/m^2 for significant power generation [14], it was found that $u > 10$ m/s for 1.9% of the time and $u > 12$ m/s for 0.36% of the time. Wind speed and direction were used in combination with peak aerodynamic coefficients on a single heliostat in the University of Adelaide wind tunnel, as a function of the elevation and azimuth tracking angles of individual heliostats in the CESA-I field. It is noted that the aerodynamic coefficients on a single heliostat are conservative for the whole field, as the loading on in-field heliostats would likely decrease due to blockage from upstream heliostats. By applying two criteria of wind speed and direction to the stowing strategy of parts of the heliostat field with similar azimuth angle rather than the whole field, the overall energy yield can be increased during synoptic high-wind periods with a steady wind direction. The operating wind loads on the heliostats that continued operating during high-wind periods were estimated using the wind load coefficients [8] corresponding to azimuth-elevation angle configuration, and comparing with the maximum stow loads to ensure the structural integrity of the supporting pylon, torque tube, drives and foundation.

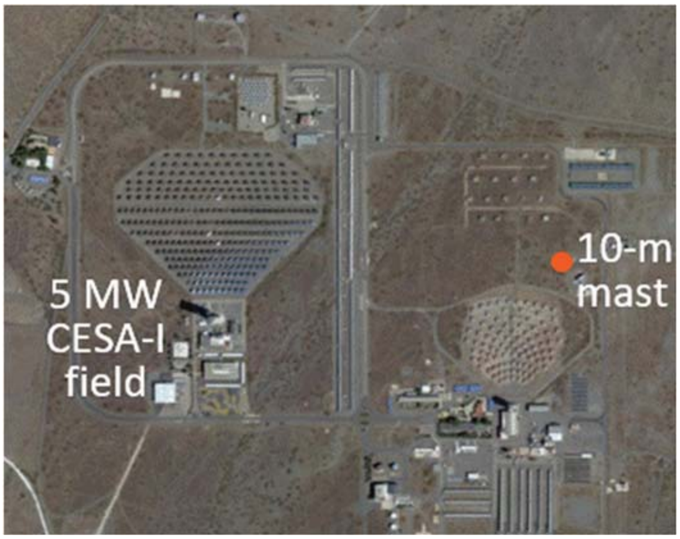

(a)

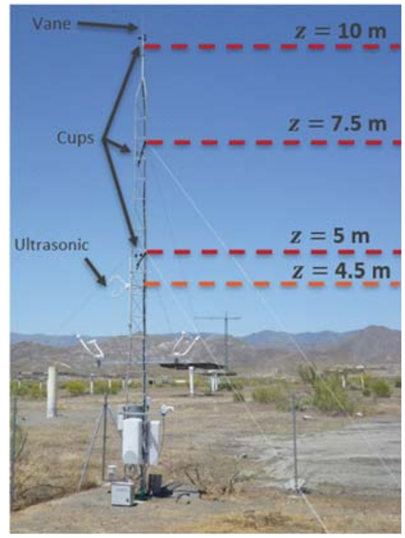

(b)

FIGURE 1. (a) Plan view of the CESA-I heliostat field and 10-m mast (Google.org), (b) meteorological mast with cup, vane and ultrasonic anemometers at different heights

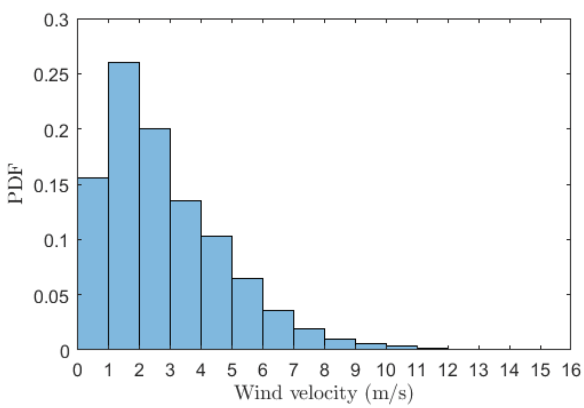

(a)

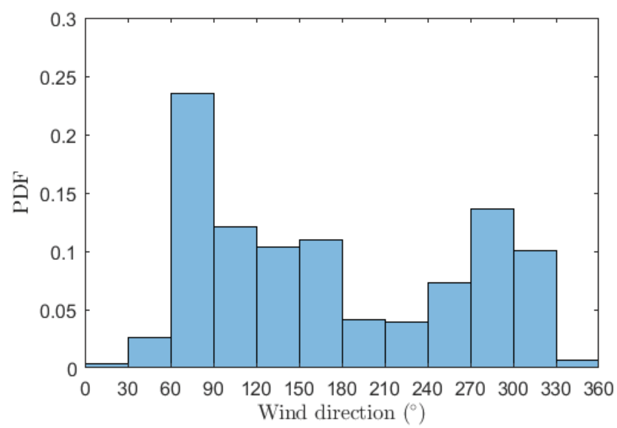

(b)

FIGURE 2. Normalised probability distributions of 1-minute-data in 2016: (a) wind speed, (b) wind direction

Figure 3 shows the distributions of heliostat tracking angles, defined as the elevation angle α with respect to the horizontal (denoted by length of arrows) and the azimuth angle (denoted by direction of arrows clockwise with respect to north), throughout the operating hours of the field on 21 June 2016. The distributions of elevation (Figure 3a) and azimuth (Figure 3b) angles are symmetric at 12:00, however there is an increased asymmetry in the afternoon at 16:00 (Figure 3c-d). Figure 3(e-f) show that the elevation angles has a smallest variation across the north-south boundaries of the field of 20° at 12:00 in summer, compared to a maximum variation of 40° at 06:00 and 18:00. During a 30 m/s gust wind speed, the hinge moment on a heliostat at an elevation angle of 45° is approximately 30% smaller than the hinge moment on a heliostat at a 30° elevation angle [7]. Furthermore, the azimuth angle shows the maximum variation of 70° across the east-west boundaries of the field at 12:00 in summer. The azimuth moment in the typical operating range of $15° \leq \alpha \leq 60°$ is reduced by more than 50% with ±15° deviation of the wind direction from the maximum azimuth load cases at $\beta = 60°$ and 120° [8]. Hence, the loading on heliostats outside of the critical range of wind directions are likely to conform to the conventional safety factor of 1.5 for high wind speed sites [15]. Hence, the largest variation of operating azimuth angles throughout the field in summer offers the greatest potential to stow only those heliostats in segments of the field excluded from (or within) a cone of acceptance of the wind direction during a high-wind (gust) event when the wind speed exceeds the design threshold.

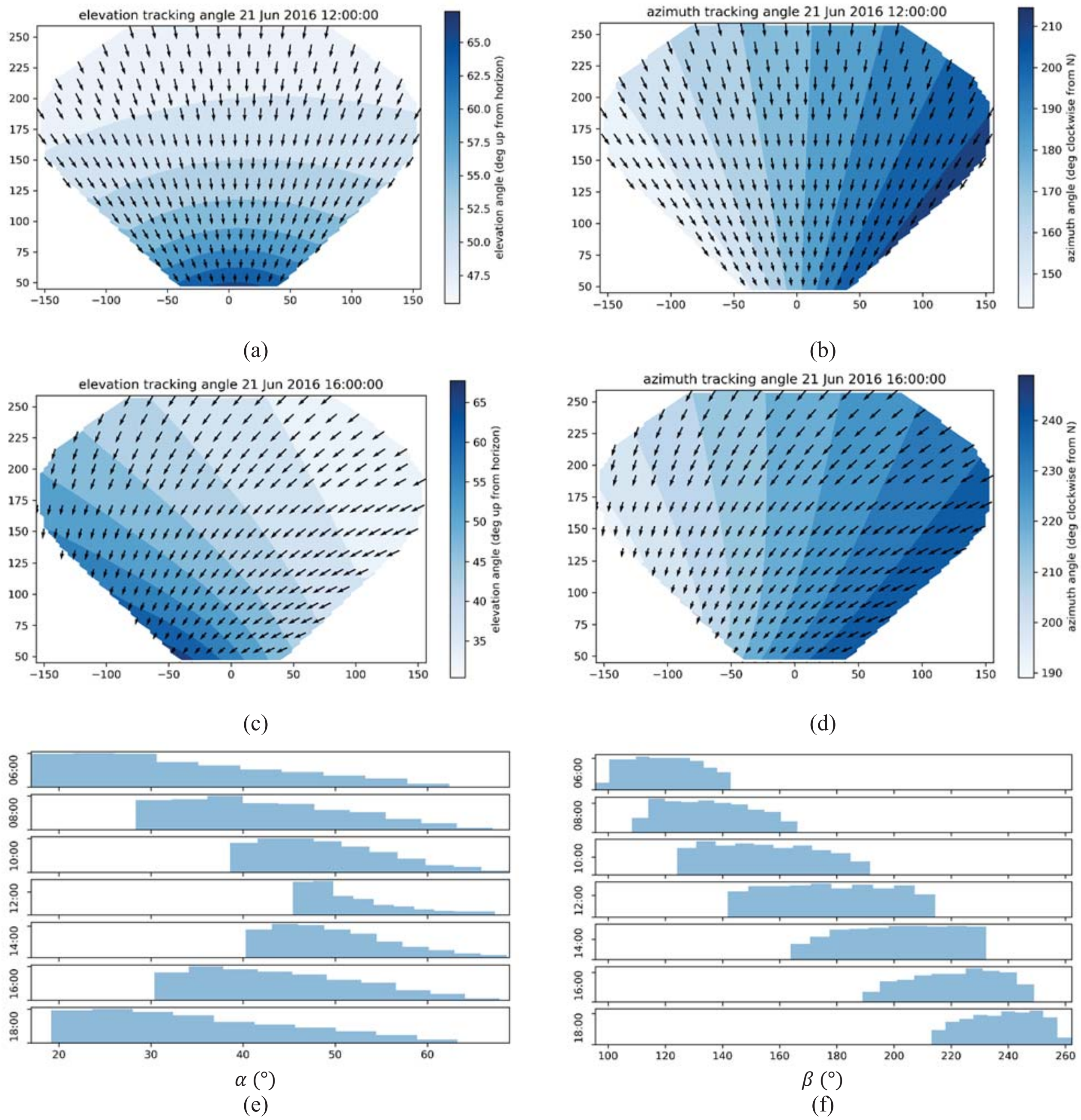

FIGURE 3. Heliostat tracking angle distributions on 21 June 2016: (a-b) elevation and azimuth angles at 12:00, (c-d) elevation and azimuth angles at 16:00, (e-f) histograms of the operating elevation and azimuth angles throughout the CESA-I field at different times throughout the day. The size of the arrows in (a-d) indicates the magnitude of the elevation angle, and the direction of the arrows indicates the azimuth angle in terms of the facing direction of each heliostat.

RESULTS AND DISCUSSION

Figure 4 shows a case study analysis of the correlations of the wind speed, wind direction and DNI on 21 June 2016 to determine the distribution of the elevation and azimuth angles of the 300 heliostats in the CESA-I heliostat field. The time series (Figure 4a) indicate a clear day with DNI approaching 1000 W/m^2 and moderate to high one-minute average easterly wind speeds above 5 m/s and exceeding 10 m/s during the maximum DNI period from 12:00

to 15:00. Correlation of the 10-minute averages of wind speed and DNI for more than two years in Figure 4(b) shows a weak correlation between wind speed and DNI. In the 3D histogram shown in Figure 4(b), the statistical occurrence of DNI against wind speed is shown by the colorbar. This frequency is indicated by the grey grid values in the maximum operating wind speed range of 5-10 m/s, where the color of each pixel shows the frequency of the bin within the DNI range (row) of the grid. With increasing DNI, there is an increased range and average value of wind speed. This is supported by the scatter plot in Figure 4(b), which shows that the median values of the DNI-weighted wind speed for day and night conditions increase from 2 m/s to 5 m/s with increasing DNI from 0 to 1100 W/m^2. Figure 4(c-d) show the distribution of the elevation and azimuth angles of individual heliostats in the CESA-I field, averaged over the minutes with $u > 10$ m/s in Figure 4(a). The elevation angle showed a small variation throughout the field, ranging from $\alpha = 39°$ in the inner field and decreasing with distance from the tower to $\alpha = 30°$, which corresponds to the maximum operating lift force and hinge moment coefficients [7]. The azimuth angle β showed a maximum variation from 77° in the eastern sector to 133° in the western sector of the field, as indicated by the red circles in Figure 4(d). This operating range of azimuth angles represents the smallest values of the hinge moment and overturning moment resisted by the torque tube and foundation, The aerodynamic wind load coefficients of smallest magnitude (close to zero) occur for wind approaching at $\beta = 90°$ perpendicular to the heliostat facing direction. However, the maximum azimuth moments occur at $\beta = 60°$ and 120°. Hence, there is a narrow margin of azimuth angles (90 ± 15°) for which the expected hinge moments and overturning moments are below 30% of their maximum load cases at $\beta = 0°$ and 180°, and the azimuth moment is below 50% of its maximum at $\beta = 60°$ and 120°. As indicated by the contour lines in Figure 4(d), there are 154 heliostats in the field within the operating range of $\beta = 90$ ± 15°. This suggests that the eastern half of the field could safely continue operation without exceeding the maximum operating load during a steady wind of constant direction that would otherwise stow the entire field upon reaching the design wind speed. Assuming the duration of the transition from the operating positions of the heliostat field to stow position is 10 minutes at the occurrence of a 10 m/s wind gust and an additional 10 minutes to return heliostats to their operating positions, the stowing strategy to allow heliostats with $\beta = 90 \pm 15°$ to continue to operate was investigated. Adopting such a strategy increased the thermal energy collected by 280 MWh through heliostat operation during periods that would conventionally stow the entire field with 24 GWh of thermal energy captured in the year 2016.

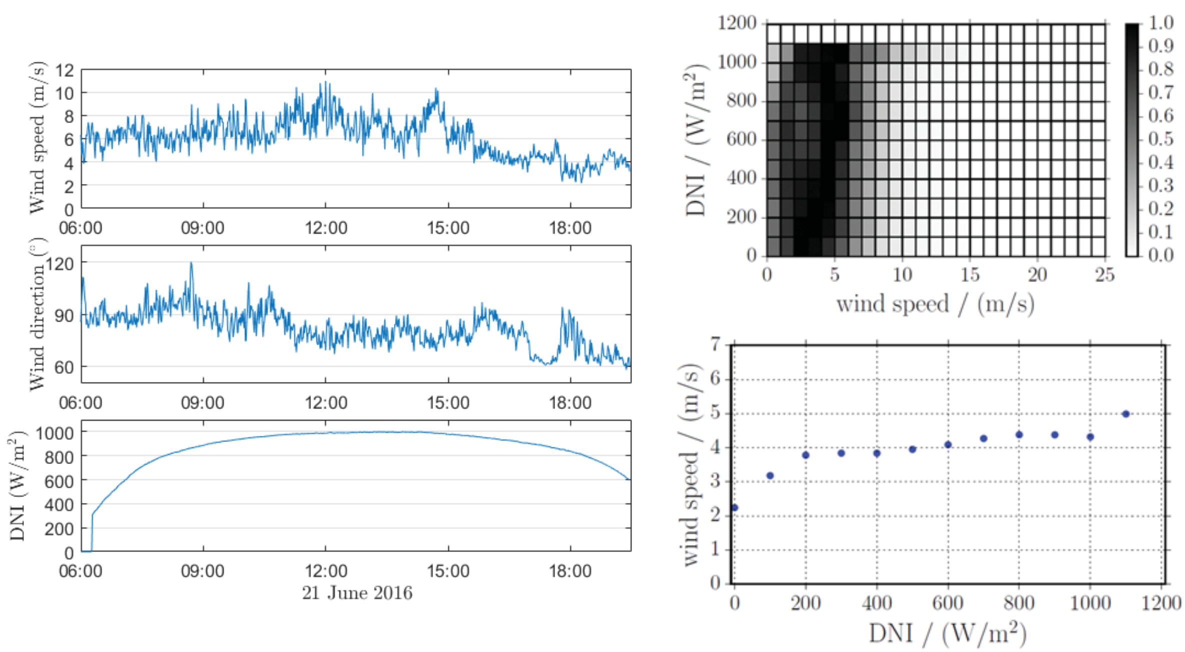

(a) (b)

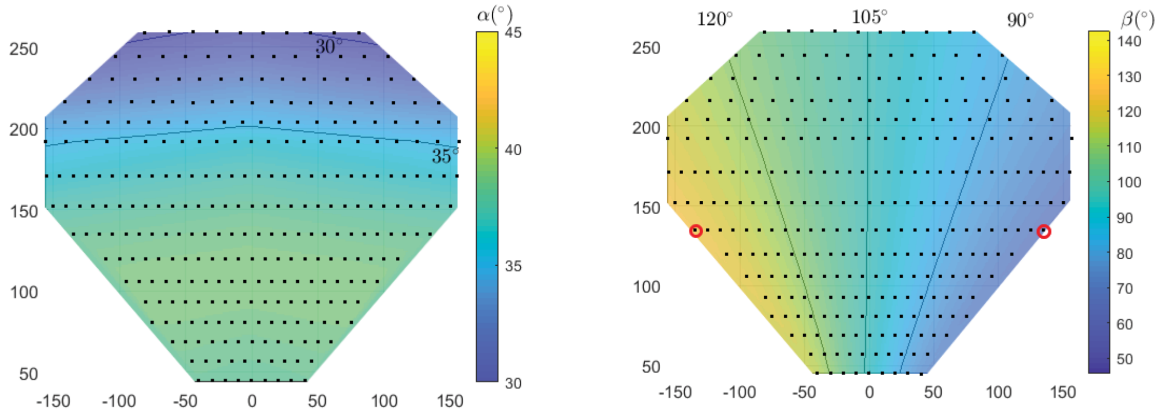

(c) (d)

FIGURE 4. Case study on 21 June 2016: (a) wind speed, direction and DNI time series, (b) correlation of 10-minute DNI-weighted wind speed and DNI. Lower plot: median of wind speed in different DNI categories. Upper plot: statistical occurrence of DNI vs. wind speed, normalized for each DNI category, (c) distribution of heliostat elevation angles at $u > 10$ m/s, (d) distribution of heliostat azimuth angles at $u > 10$ m/s. Red circles indicate the individual heliostats corresponding to the maximum and minimum azimuth angles throughout the field.

Figure 5 shows the peak operating loads on the 300 individual heliostats within the CESA-I field for the high-wind periods with $u > 10$ m/s. It can be observed in the histogram distributions with 50 Nm bins in Figure 5(a-c) that there is a wide range of operating loads throughout the heliostat field due to differences in elevation angle (Figure 4c) and particularly azimuth angle (Figure 4d) of individual heliostats. The peak hinge moments (Figure 5a) and overturning moments (Figure 5b) distributions are negatively skewed with increasing magnitude, however only 16 heliostats (5.3% of the field) are within the maximum bin range of M_{Hy} = 650-700 Nm and only 8 heliostats (2.7%) are within the maximum bin range of M_y = 1000-1050 Nm. In contrast, the peak azimuth moments (Figure 5c) are positively skewed with increasing magnitude, such that there are 27 heliostats (9%) and 49 heliostats (16.3%) of the field with peak $M_z < 50$ Nm and $M_z < 100$ Nm, respectively. Based on the ultimate design stow condition using the maximum stow aerodynamic coefficients [3, 7, 8] over all of the azimuth angles at a turbulence intensity I_u = 13%, the maximum operating loads on the individual heliostats in Figure 5(d-f) were normalized against the stow design wind loads. The results confirm that the loading distribution for this high-wind period in summer are highly dependent on the azimuth angle of individual heliostats in the field. The normalized hinge moments (Figure 5d) and overturning moments (Figure 5e) are largest in the western sector of the field, reaching maximum values of 37% and 22% of the stow load, respectively, compared to minimum values of 1% and 7% in the eastern sector of the field. The peak operating azimuth moments (Figure 5f) exceed the stow load by up to a factor of 2.5 in the western sector of the field, due to the considerably smaller azimuth moment coefficients in stow [3]. However, there are 69 heliostats (23%) in the eastern sector of the field with azimuth moments below 50% of the stow azimuth moment. Hence, this indicates that there is a significant variation in the peak operating loads throughout a heliostat field based on azimuth angle, which are considerably lower than the stow design load within a safety factor of at least 1.5. Furthermore, adopting a stowing strategy based on wind load offers an effective and robust solution to stow only those individual heliostats (or rows) in the field that exceed the maximum operating design load and ultimate design stow load specifications. Instrumentation of heliostats in different rows within a field would also be highly beneficial to better understand the wind-blocking and vortex shedding effects on the heliostat field aerodynamics and wind load distributions.

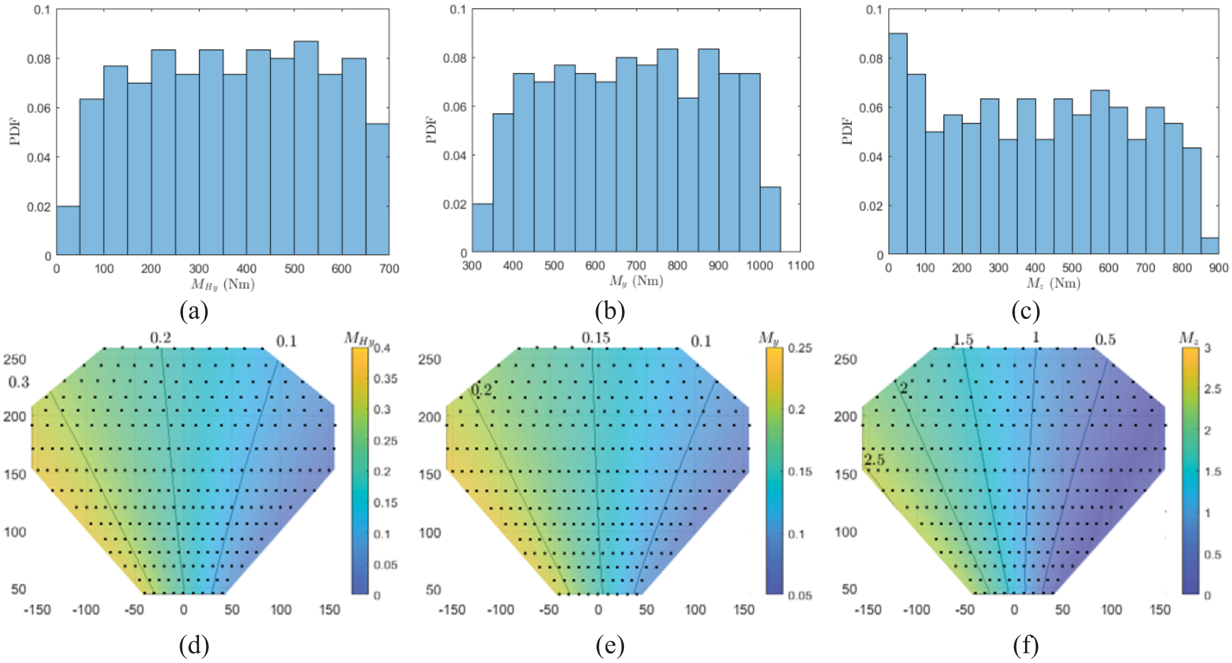

FIGURE 5. Distributions of the peak operating load throughout the CESA-I heliostat field at $u > 10$ m/s on 21 June 2016 and relative to the stow load: (a,d) hinge moment, $M_{Hy,stow} = 1884$ Nm, (b,e) overturning moment, $M_{y,stow} = 4587$ Nm, (c,f) azimuth moment $M_{z,stow} = 344$ Nm.

Figure 6 shows the operating time of the CESA-I field, normalized with respect to the operating minutes with $DNI > 300$ W/m^2 by season in 2016. Based on the results in Figures 4 and 5, those heliostats in the field with $\beta = 90 \pm 15°$ are assumed to operate at wind speeds larger than the stated stow design wind speed. As the maximum allowed wind speed is increased from 6 m/s to 12 m/s, the operating time increases by 7% in winter and summer, 6% in spring and 2% in autumn. An increase of 6% of the annual operating time of the heliostat field can thus be achieved by continuing to operate above the maximum operating design wind speed, only for those heliostats in the field within the stated range of azimuth angles. This indicates that there is a significant opportunity to increase the annual performance and efficiency of a heliostat field through the adoption of a partial stowing strategy of a heliostat field, based on wind speed and direction. It should be noted that the estimated peak wind loading distributions on single heliostat aerodynamic coefficients provide a conservative measure of the loading distribution throughout the heliostat field. Further work to verify a stowing strategy based on wind direction, or wind load, should consider the blockage and vortex shedding of heliostat-induced wake turbulence and the resulting variation of wind loads on heliostats in different rows. Partial operation of the field would also need to verify the benefit and/or limitation to the optical performance of the heliostat field and the aiming distribution and heat flux profiles over the surface of the receiver.

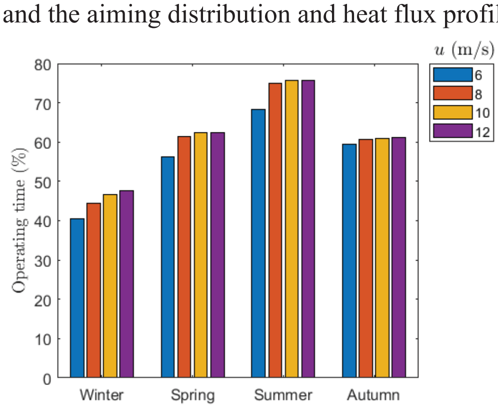

FIGURE 6. Operating time by season, relative to all operating minutes with $DNI > 300$ W/m^2 in 2016, of the CESA-I heliostat field, including operating heliostats with $\beta = 90 \pm 15°$ at wind speeds larger than the stated maximum wind speeds

CONCLUSIONS

This paper investigated a stowing strategy of a heliostat field based on wind speed and direction, in terms of the potential benefit of additional operating minutes and energy generation through the partial stowing of only individual heliostats within a cone sector of $\beta = 90 \pm 15°$ representing the range of minimum operating wind loads. The results show that partial stowing of the field through reduced wind loading of some regions of the field due to differences in azimuth angle can achieve increased operating time of the heliostat field. For example, up to 23% of heliostats in the eastern sector of the field have a peak operating azimuth moment with magnitude less than 50% of the stow azimuth moment, with the operating hinge and overturning moments remaining less than 10% of their respective stow load cases. As the stow design wind speed is increased from 6 m/s to 12 m/s, the annual operating minutes of the plant can be increased by 6% throughout the year by adopting a stowing strategy to allow heliostats with $\beta = 90 \pm 15°$ to continue to operate. It was found that employing this stowing strategy at wind speeds exceeding 10 m/s can achieve an additional 280 MWh of thermal energy collected by heliostat field operation in a year, which would conventionally stow the entire field with 24 GWh of annual thermal energy captured.

ACKNOWLEDGMENTS

Support for the work has been provided by the Australian Solar Thermal Research Institute (ASTRI) through funding provided by the Australian Renewable Energy Agency (ARENA). The authors would also like to acknowledge the contribution of wind data analysis in an internal project report by Natalie Hanrieder, DLR, and the coordinate system of the CESA heliostat field provided by Jesús Fernández-Reche, PSA.

REFERENCES

1. G. J. Kolb, C. K. Ho, T. R. Mancini and J. A. Gary, *Power tower technology roadmap and cost reduction plan* (Sandia National Laboratories, Albuquerque, (2011), SAND2011-2419.
2. A. Pfahl, J. Coventry, M. Röger, F. Wolfertstetter, J. F. Vásquez-Arango, F. Gross, M. Arjomandi, P. Schwarzbözl, M. Geiger and P. Liedke, "Progress in heliostat development," *Solar Energy* **152**, pp. 3-37 (2017).
3. M. J. Emes, A. Jafari, J. Coventry and M. Arjomandi, "The influence of atmospheric boundary layer turbulence on the design wind loads and cost of heliostats," *Solar Energy* **207**, pp. 796-812 (2020).
4. M. Burisch, A. Mutuberria, D. Olasolo and C. Villasante, "Influence of limited heliostat motion onto the efficiency of a solar field," in *AIP Conference Proceedings*,(AIP Conference Proceedings, 2016), 020004.
5. J. Vásquez-Arango, "Dynamic Wind Loads on Heliostats," PhD Thesis, DLR, Uni Aachen, 2016.
6. A. Zeghoudi and A. Chermitti, "Estimation of the Solar Power Tower Heliostat Position using Neural Network," *International Journal of Computer Applications* **94**, pp. 41-46 (2014).
7. M. J. Emes, A. Jafari, F. Ghanadi and M. Arjomandi, "Hinge and overturning moments due to unsteady heliostat pressure distributions in a turbulent atmospheric boundary layer," *Solar Energy* **193**, pp. 604-617 (2019).
8. M. J. Emes, A. Jafari and M. Arjomandi, "Wind Load Design Considerations for the Elevation and Azimuth Drives of a Heliostat," in *SolarPACES* (SolarPACES, Daegu, 2019).
9. M. J. Emes, M. Arjomandi, F. Ghanadi and R. M. Kelso, "Effect of turbulence characteristics in the atmospheric surface layer on the peak wind loads on heliostats in stow position," *Solar Energy* **157**, pp. 284-297 (2017).
10. M. Arjomandi, M. Emes, A. Jafari, J. Yu, F. Ghanadi, R. Kelso, B. Cazzolato, J. Coventry and M. Collins, "A Summary of Experimental Studies on Heliostat Wind Loads in a Turbulent Atmospheric Boundary Layer," in *SolarPACES* (SolarPACES, Daegu, 2019).
11. A. Jafari, M. Emes, B. Cazzolato, F. Ghanadi and M. Arjomandi, "An Experimental Investigation of Unsteady Pressure Distribution on Tandem Heliostats," in *SolarPACES* (SolarPACES, Daegu, 2019).
12. A. Jafari, F. Ghanadi, M. Arjomandi, M. J. Emes and B. S. Cazzolato, "Correlating turbulence intensity and length scale with the unsteady lift force on flat plates in an atmospheric boundary layer flow," *Journal of Wind Engineering and Industrial Aerodynamics* **189**, pp. 218-230 (2019).
13. N. Hanrieder, *WP1 - Wind data-Analysis* internal project report, MAHWIN project, 0324213B, DLR, 2017).
14. Z. Wang, "Chapter 2 - The Solar Resource and Meteorological Parameters," in: Z. Wang (Ed.) *Design of Solar Thermal Power Plants*, Academic Press, 2019, pp. 47-115.
15. J. B. Blackmon, "Heliostat drive unit design considerations–Site wind load effects on projected fatigue life and safety factor," *Solar Energy* **105**, pp. 170-180 (2014).